

Final report about the NKFIH-OTKA (K-132568) project

entitled

“NaCl-induced inhibition of the photosynthetic functions and growth of microalgae and plants in interaction with other stress factors (drought and strong light)”

The project concentrated on the following main topics:

- 1, Mechanism of NaCl-induced inhibition of photosynthetic functions in microalgae with special emphasis on the widely used model cyanobacterium *Synechocystis* PCC 6803.
- 2, The effect of NaCl-induced stress, alone or in combination with drought, on the growth and photosynthetic activity in higher plants.

Main findings:

- 1, Mechanism of NaCl-induced inhibition of photosynthetic functions in microalgae with special emphasis on the widely used model cyanobacterium *Synechocystis* PCC 6803.

We aimed to identify the inhibitory sites of NaCl in the whole photosynthetic electron transport in *Synechocystis* sp. PCC 6803 WT cells by using multiple biophysical tools. Exposure of cells to various NaCl concentrations (200 mM to 1 M) revealed the inhibition of Photosystem II (PSII) activity at the water oxidizing complex and between the Q_A and Q_B electron acceptors. In contrast to the inhibition of PSII, electron flow through Photosystem I (PSI) was accelerated indicating enhanced cyclic electron flow. Our data show that the enhanced cyclic electron flow is mediated, at least partly, via the NDH-1 complex. To study this process we established a new experimental approach, which is based on the detection of the so-called AG thermoluminescence band (Kodru et al. *Physiologia Plant.* 171, 291-300, 2021).

Importantly, the oxygen-evolving capacity of the cells was inhibited to a larger extent when only CO_2 was the final electron acceptor in the Calvin-Benson-Bassham (CBB) cycle than in the presence of the PSII electron acceptor DMBQ suggesting important NaCl inhibitory site(s) downstream of PSI. Measurements of NADPH kinetics revealed NaCl-induced inhibition of light-induced production of NADPH as well as retardation of NADPH consumption both in the light and in the initial dark period after switching off the light. Chlorophyll fluorescence kinetics, measured in parallel with NADPH fluorescence, showed the enhancement of post-illumination fluorescence rise up to 500 mM NaCl, which was however inhibited at higher NaCl concentrations. Our results show, for the first time, that NaCl inhibits the activity of the CBB cycle at least at two different sites and confirm earlier results about the NaCl-induced inhibition of the PSII donor and acceptor side and the enhancement of electron flow through PSI.

An accepted manuscript about the results is under publication in *Physiologia Plantarum* (the whole manuscript is attached at the end of the report). Salt-induced inhibition of CO_2 fixation by the CBB cycle was also confirmed by direct CO_2 measurements using Membrane Inlet Mass Spectrometer (MIMS) device (MS-GAS 100, Photon Systems Instruments), which allows the detection of gases and other volatile compounds up to 100 mass numbers in aqueous and gas-phase environments.

The NaCl-induced inhibition of PSII electron transport and the involvement of the CBB cycle (inhibition of NADPH utilization) were also demonstrated in the green algae *Chlorella sorokiniana* and *Chlamydomonas reinhardtii*.

As regards the interaction of NaCl- and high-light-induced stress, we demonstrated that the gene expression induced by the formation of singlet oxygen ($^1\text{O}_2$) caused by bright light shows a partial overlap with the NaCl-induced gene expression in *Synechocystis* 6803 (Patyi et al. *Physiologia Plant*, 176, 1-20, 2024). This finding suggests that the NaCl-induced expression of the affected genes may be mediated by $^1\text{O}_2$.

2, The effect of NaCl-induced stress, alone or in combination with drought, on the growth and photosynthetic activity in higher plants.

One of our foci was to evaluate the interaction of salt (2 and 3 g NaCl/kg soil) and drought stress (20 % relative soil humidity) in various lines of tomato lines. One of the experimental objects was a set introgression lines, between salt-tolerant wild *Solanum pennellii* and the cultivated *Solanum lycopersicum*. The effect of these stress factors, alone and in combination, was followed by the application of a high throughput plant phenotyping platform, which monitors not only the growth of green parts (shoots/leaves), but also the root structure. The experiments were repeated three times, up to four months each, following the plants until fruit production and final harvest. The results show that the IL7-4-1 and IL8-3 introgression lines show a higher degree of salt tolerance in terms of biomass accumulation than the M82 control line. Interestingly and unexpectedly, we observed a small increase in biomass in the presence of 2 and 3 g/kg salt in all three lines instead of the expected decrease in biomass in the control. In the case of fruit formation, increasing soil salinity in the IL7-4-1 and IL8-3 lines resulted in a decrease in yield, but in the case of the IL2-5 line, the highest yield was observed at the highest (3g/kg) soil salinity. Drought stress (20% relative soil moisture) alone caused a significant decrease in the amount of fresh and dry biomass and completely inhibited fruit (berry) development in the control and the three introgression lines. The combination of elevated soil salinity and reduced soil moisture only slightly reduced biomass, but fruit formation was only observed in the IL8-3 line at 3g/kg salt at 20% relative soil moisture. These data suggest that the introgression tomato lines not only show increased salt tolerance compared to the control line, but also show a small stimulation of both biomass and fruit production at the applied soil salinity of 2 and 3 g/kg. From the data a publication is under preparation with the collaboration partner (Prof. Anne Frary, Ismir Institute of technology, Turkey).

We also investigated the response of salt tolerant tomato landraces to salt and drought stress originating from saline zones of Bihor County, in North-Western Romania in cooperation with the group of dr. Cosmin Sicora from the Biological Research Centre, Jibou, Romania. Phenotypic characterization of collected landraces provided information regarding the resistance to drought and salt stress compared with Marmande cultivar. Root density, leaf area and the reaction under different concentrations of salt and different water content were compared to conclude which landraces are more suitable for future genotypic studies to use them in breeding programs. The aim is to obtain genotypes with increased drought and salt stress resistance to improve crop yield and quality in saline environments. This study highlights the potential of local tomato landraces from Bihor County as valuable genetic resources for developing resilient varieties that can thrive in challenging environmental conditions. The results are submitted for publication to a horticultural journal.

Another important cultivated plant species whose salt-tolerance is important is tomato. To maintain a sustainable potato production, it is necessary to develop stress tolerant potato cultivars that cope with the already ongoing climate change. We tested somatic hybrid lines generated by the group of Prof. Elena Tyca-Rakosy at the University of Cluj-Napoca by electrofusion of cultivated *Solanum tuberosum* and wild *Solanum chacoense* potato protoplasts and plant regeneration, with or without mismatch repair deficiency (MMR). Upon this selection of drought and salt tolerant genotypes, somatic hybrids and their parents were phenotyped on a semi-automated platform, and lines tolerant to medium water scarcity (20% compared to 60% soil water capacity) were identified. Although none of the parental species were tolerant to drought, some of the MMR-deficient somatic hybrids showed tolerance to drought and salt as a new trait. The results were published (Molnár et al., Agriculture 11, 696, 2021). An extension of these experiments were performed with additional somatic hybrid lines under co-occurring salt- and drought stress, the publication of the results is under preparation.

We aimed to test the hypothesis that NaCl may also have a direct inhibitory site in the Calvin-Benson-Bassham cycle in higher plants. To this end, we attempted NADPH kinetic studies in intact tomato and potato leaves. Unfortunately, the NADPH fluorescence measurement method that works well in algal cultures did not give evaluable results in tomato or potato leaves, probably due to the morphological characteristics of the leaves.

On the other hand, parallel measurements of NADPH and Chl fluorescence kinetics gave promising preliminary results in salt-stressed *Arabidopsis* leaves, which point to the existence of direct NaCl-induced inhibition of the CBB cycle in higher plants. However, full completion of these measurements will require further experimental optimization, which will be performed in the follow-up of the OTKA project.

Manuscript accepted in *Physiologia Plantarum* (in print)

Editorial decision: Accept (23 December, 2024)

PPL-2024-01701-ePSII11.R1 -

"Investigation of the effect of salt stress on photosynthetic electron transport pathways in the *Synechocystis* PCC 6803 cyanobacterium"

Author(s): Patil, Priyanka Pradeep; Kodru, Sandeasha; Szabó, Milán; Vass, Imre

Dear Imre,

After reading your manuscript and your answer to the reviewers' comments, I am pleased to accept your manuscript for publication. For your information, the reviewers' comments (if any) are included below.

You will shortly be contacted by the editorial office staff, who will ensure that your manuscript is fit for article production. The editorial office will work together with the authors to deliver the best possible version of your article.

Yours sincerely,
Physiologia Plantarum Editorial Office

Investigation of the effect of salt stress on photosynthetic electron transport pathways in the *Synechocystis* PCC 6803 cyanobacterium

Priyanka Pradeep Patil^{1,2}, Sandeasha Kodru^{1,2}, Milán Szabó¹ and Imre Vass^{1*}

¹ Institute of Plant Biology, HUN-REN Biological Research Centre, 6726 Szeged, Hungary

² Doctoral School of Biology, Faculty of Science and Informatics, University of Szeged, 6720 Szeged, Hungary

* Corresponding authors
E-mail: vass.imre@brc.hu (IV)

Abstract

Cyanobacteria are important model organisms for studying the process of photosynthesis and the effects of environmental stress factors. This study aimed to identify

the inhibitory sites of NaCl in the whole photosynthetic electron transport in *Synechocystis* sp. PCC 6803 WT cells by using multiple biophysical tools. Exposure of cells to various NaCl concentrations (200 mM to 1 M) revealed the inhibition of Photosystem II (PSII) activity at the water oxidizing complex and between the Q_A and Q_B electron acceptors. In contrast to the inhibition of PSII, electron flow through Photosystem I (PSI) was accelerated indicating enhanced cyclic electron flow. The oxygen-evolving capacity of the cells was inhibited to a larger extent when only CO₂ was the final electron acceptor in the Calvin-Benson-Bassham (CBB) cycle than in the presence of the PSII electron acceptor DMBQ suggesting important NaCl inhibitory site(s) downstream of PSI. Measurements of NADPH kinetics revealed NaCl-induced inhibition of light-induced production of NADPH as well as retardation of NADPH consumption both in the light and in the initial dark period after switching off the light. Chlorophyll fluorescence kinetics, measured in parallel with NADPH fluorescence, showed the enhancement of post-illumination fluorescence rise up to 500 mM NaCl, which was however inhibited at higher NaCl concentrations. Our results show, for the first time, that NaCl inhibits the activity of the CBB cycle at least at two different sites, and confirm earlier results about the NaCl-induced inhibition of the PSII donor and acceptor side and the enhancement of electron flow through PSI.

Keywords: Salt stress, Photosystem I and II, NDH-1 complex, *Synechocystis* sp. PCC 6803, Calvin-Benson-Bassham cycle

1 INTRODUCTION

Salt stress is an important phenomenon, that affects higher plants, as well as freshwater microalgae, including cyanobacteria (Lu & Vonshak, 1999; Allakhverdiev & Murata, 2008; Gong *et al.*, 2008; Yang *et al.*, 2020). Cyanobacteria have a photosynthetic system similar to that of higher plants therefore they can be used as model systems to study the mechanisms of photosynthesis in general and under various stress conditions.

The photosynthetic process is mediated by large pigment-protein complexes embedded in the thylakoid membrane and soluble electron transfer carriers in the thylakoid lumen and the cytosol. The membrane-bound components are Photosystem II (PSII), which performs light-induced water oxidation serving as the initial electron donor of photosynthetic electron transport, Photosystem I (PSI) which elevates the electrons arriving from PSII to highly reducing potential to produce NADPH as a reducing agent utilized in downstream processes. The *cytb₆f* complex together with the thylakoid-lumen-located plastocyanin (PC), or cytochrome *c₆* (Cyt_{c₆}), mediate the electron transport between the two photosystems. Light-induced electron transfer in PSII drives water oxidation via the water oxidizing complex (WOC) with a tetra-manganese cluster as a catalytic site. The electrons liberated from water oxidation are transferred from the donor side of PSII, via a redox-active tyrosine (Tyr-Z), and the primary electron donor Chl assembly (P680) to the primary electron acceptor pheophytin (Phe) where from it is transferred to a protein-bound plastoquinone molecule (Q_A) acting as the first quinone electron acceptor (see (Cardona *et al.*, 2012)). Reduced Q_A can be reoxidized by a second plastoquinone electron acceptor called Q_B which is a mobile electron carrier. PQ molecules can bind in their oxidized form to the Q_B binding site and act as a two-electron acceptor. After receiving the first electron from Q_A⁻ the single-reduced Q_B⁻ is stable in the binding site, but after the second reduction and subsequent protonation the double reduced quinol (QBH₂) form can leave the binding site and deliver the electrons to a pool of PQ molecules located in the lipid phase of the thylakoid membrane, see (Crofts & Wraight, 1983). From the PQ pool the electrons are delivered via plastocyanine (PC) to the donor side of PSI where they re-reduce the oxidized primary electron donor of PSI, called P700⁺, which is produced by light-induced charge separation in PSI leading to the transfer of an electron to the acceptor side of PSI. At the PSI acceptor side ferredoxin (Fd) acts as a central hub for electron distribution towards downstream processes, primarily the production of NADPH via ferredoxin Fd-NAD(P)H-oxidoreductase (FNR), as well as cyclic electron transport back to the PQ pool.

The electron transport through PSII and the *cytb₆f* complex is coupled with trans-thylakoid proton translocation, and the produced proton gradient is utilized in ATP synthesis by the action of the membrane-bound ATP-synthase. The NADPH and ATP molecules produced in the light-dependent phase of photosynthetic electron transport are utilized in various downstream processes, most importantly in CO₂ reduction in the Calvin-Benson-Basham (CBB) cycle, using CO₂ as the final electron acceptor in the photosynthetic process.

Inhibitory effects of salt stress on photosynthetic electron transport have been studied for several decades, revealing multiple inhibitory sites' existence. However, the results obtained by different research groups are partly contradictory and no consensus picture has emerged yet concerning the exact location of the inhibitory sites and their importance in the overall salt stress effect, for reviews see (Sudhir & Murthy, 2004; Allakhverdiev & Murata, 2008; Yang *et al.*, 2020), and no consensus picture has emerged yet concerning the exact location of the inhibitory sites and their importance in the overall salt stress effect.

The main points of contradiction concern the sites of salt-induced inhibition of PSII activity since the donor side (Allakhverdiev *et al.*, 2000; Allakhverdiev & Murata, 2008), the acceptor side (Gong *et al.*, 2008) as well as the reaction center complex (Lu & Vonshak, 1999) were all suggested. Another unresolved topic is the effect of salt on PSI activity since

both a ca. 50 % inhibition (Allakhverdiev *et al.*, 2000) and 80% enhancement were reported (Lu & Vonshak, 1999). This contradiction could possibly be related to the enhancement of cyclic electron transport around PSI, which was reported by different authors.

An additional hiatus in our knowledge is the possible salt-induced inhibition of electron transport downstream of PSI. This effect has not been reported yet, but direct salt-induced inhibition of some key enzymes of the CBB cycle (Yang *et al.*, 2008; Pan *et al.*, 2021), which performs CO₂ reduction by using electrons arriving from water oxidation, points to this possibility.

Our work aimed to perform a comprehensive study of NaCl-induced inhibition of electron transport in the whole photosynthetic electron transport chain starting from H₂O oxidation in PSII, through PSI and cyclic processes, until the CBB cycle where CO₂ reduction acts as the final electron acceptor. Our data confirm salt-induced inhibition of the water oxidation process at the PSII donor side, partial inhibition of the Q_A⁻ to Q_B electron transfer at the PSII acceptor side, as well as increase of cyclic electron flow around PSI. In addition, our results demonstrate that the main inhibition of photosynthetic electron transport by salt stress occurs downstream of PSI indicating at least two different inhibitory sites in the CBB cycle.

2 MATERIALS AND METHODS

2.1 Cell culture, growth conditions

Synechocystis sp. PCC 6803 WT (referred to as *Synechocystis*) cells were grown autotrophically in the presence of 3% CO₂, at 40 μmol photons m⁻² s⁻¹ and 30°C. Cells were suspended in 500 mL Erlenmeyer flasks containing the final volume of 200 mL BG-11 medium placed on a rotary shaker (GALLENKAMP, Cambridge, United Kingdom). For measurements cells were harvested in their early exponential growth phase OD_{720nm} = 0.8-1, centrifuged at 6500xg for 6 min, then resuspended in fresh medium to adjust the chlorophyll a (Chl) content to 5 μg mL⁻¹. Chl content was determined using UV-visible spectrophotometer (UV-1601, Shimadzu corporation, Japan) by methanol extraction method (see (Patil *et al.*, 2020)).

2.2 Salt treatment

Cells were incubated with four concentrations (200 mM, 500 mM, 700 mM and 1M) of NaCl for 1 h in the incubator under growth conditions. Each sample was dark adapted for 3 min prior to every measurement described below.

2.3 Oxygen evolution measurement

Oxygen evolution and uptake rates were measured by using a Hansatech DW2 O₂ electrode (Hansatech Instruments Ltd, England). 1 mL culture (at 5 μg mL⁻¹ Chl concentration) was transferred into the reaction chamber and dark-adapted for 3 min under constant stirring at 30°C before the measurement. O₂ evolution rates were measured using a protocol consisting of a 2-minute dark period followed by a 2-minute light period. The light-dependent oxygen evolution rate was calculated as the difference between the oxygen consumption rate in the dark and the oxygen production rate in the light. For the light phase the cells were illuminated at 1000 μmol photons m⁻² s⁻¹ with white light provided by a fiber optic light source from one side of the chamber (Schott KL 1500, Schott AG, Germany). For the quantification of light-induced O₂ evolution rate the measurements were performed either without an added acceptor, representing whole chain electron transport from H₂O to CO₂ fixed by the Calvin-Benson-Bassham (CBB) cycle, or in the presence of 0.5 mM DMBQ as an artificial electron acceptor, representing PSII activity (Rehman *et al.*, 2013).

2.4 OJIP Chlorophyll fluorescence transient measurement

The OJIP Chl fluorescence transient, also called as Kautsky induction curve, was measured using an FL-3000 fluorimeter (Photon Systems Instruments, Brno, Czech Republic). Characteristic points of the fluorescence transient between the dark- to the light-adapted state are the O (F_o at 20 μ s) representing the open state of all PSII reaction centers in the dark, the maximum fluorescence intensity (P or F_m , at \sim 300 ms) corresponding to the closed state of PSII. The J and I are the two intermediate steps obtained at approximately 2 ms and 20 ms, respectively (Kalaji *et al.*, 2016). A 3s OJIP script was used for the measurement using red actinic light (650 nm at peak, spectral line half-width, 22 nm) with 3500 μ mol photons $m^{-2} s^{-1}$.

2.5 Flash-induced chlorophyll fluorescence yield relaxation kinetics

Flash-induced increase and subsequent decay of Chl fluorescence yield was measured using a double-modulation fluorometer (FL-3000, Photon System Instruments, Brno, Czech Republic) (Trtilek *et al.*, 1997). A 2 mL sample was placed in a cuvette with a 1 cm optical pathlength and was stirred with a small magnetic bar in the dark. Four measuring flashes (8 μ s, separated with 200 μ s intervals, wavelength of 620 nm) were applied to determine minimum fluorescence in the dark (F_o), after which a single turnover saturating actinic flash (30 μ s, wavelength of 639 nm) was applied that transfers the electron from the water oxidizing complex to Q_A , which results in the rise of fluorescence intensity (denoted as F_m (ST)) due to the increased yield of Chl fluorescence in the presence of Q_A^- . The relaxation of Chl fluorescence yield resulting from the reoxidation of Q_A^- was measured by applying weak, non-actinic, measuring flashes in the time range from 150 μ s to 100 s on a logarithmic time scale. Flash-induced fluorescence relaxation curves were analyzed, to determine the time constants of the fast, middle and slow phases, as well as their relative amplitudes, as described by (Vass *et al.*, 1999).

2.6 Light intensity dependence of ETR(I) and ETR (II)

Variable Chl fluorescence from PSII and the amount of oxidized PSI primary electron donor ($P700^+$) were simultaneously measured using a DUAL-PAM-100 system (HeinzWalz, Effeltrich, Germany). From the fluorescence data F_v/F_m , and the effective quantum yield of photochemical energy conversion in PS II, $Y(II) = (F_m' - F) / F_m'$ were calculated (Genty *et al.*, 1989) where F_m and F_m' is the maximal fluorescence yield from dark- and light-adapted samples, respectively.

The $P700^+$ signal may vary between a minimal ($P700$ fully reduced) and a maximal level ($P700$ fully oxidized). The maximum level of $P700^+$ is called P_m in analogy with F_m . It was determined by using a saturation pulse (300 ms, 10,000 μ mol photons $m^{-2} s^{-1}$; 635 nm) after pre-illumination with far-red light. P_m' is analogous to the fluorescence parameter F_m' and was determined by applying 800 ms saturating pulse of 635 nm red light. The photochemical quantum yield of PSI, $Y(I)$ is the quantum yield of photochemical energy conversion in PSI. It is calculated as $Y(I) = (P_m' - P) / P_m'$. $Y(ND)$ is the quantum yield of non-photochemical energy dissipation in PSI due to donor side limitation, $Y(ND) = P / P_m'$. $Y(NA)$ is the quantum yield of non-photochemical energy dissipation due to acceptor side limitation in PSI, $Y(NA) = (P_m - P_m') / P_m'$, and $Y(I) + Y(ND) + Y(NA) = 1$ (Klughammer & Schreiber, 1994).

The electron transport rates through PSII and PSI were calculated by using the formulas

$ETR(II) = Y(II) * PPF * 0.84 * 0.5$ and $ETR(I) = Y(I) * PPF * 0.84 * 0.5$ (Genty *et al.*, 1989; Schreiber *et al.*, 2012), where $Y(II)$ and $Y(I)$ are the effective quantum yields of

PSII and PSI, respectively, PPFD is photon flux density of incident photosynthetically active radiation, the two coefficients (0.5 and 0.84) imply that PSII and PSI are equally excited, and that due to sample absorbance properties only 84% of incident irradiance will be absorbed by the photosystems, respectively (Björkman & Demmig, 1987; Schreiber, 2004).

2.7 P700⁺ Reduction kinetics

The P700⁺ kinetics were measured using the DUAL-PAM-100 Chl fluorometer (Heinz Walz, Effeltrich, Germany). The Measuring Head with P700 NIR Emitter (Dual-E) and the Measuring Head with Detector (Dual-DB) were arranged opposite to each other (same as the setup used for measurements of leaves). Cells were syringe-filtered to a GF/C filter paper, which was then placed in between two coverslips with a spacer and mounted to the emitter-detector unit as described above. The redox change of P700 was measured as the difference absorbance measured at 830 nm minus the reference at 870 nm. The light-induced P700 changes were measured using a protocol that consisted of an initial 5 s dark period, followed by non-saturating Far-Red (FR) illumination (720 nm) for 20 s to oxidize P700, a saturating 20 ms flash at 25 s to determine the maximum amplitude of P700⁺ (denoted as P_m), and a dark period after switching off the FR light at 45 s to monitor P700⁺ re-reduction for additional 10 s in darkness. The ST flash caused a transient reduction of P700⁺ due to the electron flow from PSII, which was followed by a re-oxidation of P700 (the FR background light was on during and after the ST flash for the indicated time). The Chl concentration was adjusted to 40 µg for P700 measurements.

2.8 NADPH and chlorophyll fluorescence measurements

NADPH kinetics were measured using the NADPH/9-AA module of DUAL-PAM Chl fluorometer (Heinz Walz, Effeltrich, Germany) at 30°C (Schreiber & Klughammer, 2009; Kauny & Setif, 2014) in parallel with Chl fluorescence. NADPH fluorescence was excited by UV-A (365 nm) from the DUAL-ENADPH unit and detected by a blue-sensitive photomultiplier with a filter transmitting light between 420 and 580 nm in the DUAL-DNADPH unit. A slow induction measuring protocol was initiated and the NADPH/Chl fluorescence signals were recorded for 30 s in the dark having a weak measuring light (ML) of approximately 0.1 µmol photons m⁻² s⁻¹, then the actinic red light (635 nm peak intensity) at ~56 µmol photons m⁻² s⁻¹ (or near the growth light intensity) was switched on to record light-induced NADPH/Chl fluorescence change for 180 s, and subsequently the NADPH/Chl fluorescence change from light-to-dark was monitored up to 300 s (Patil *et al.*, 2020).

2.9 Data processing

Graphs were plotted and analyzed using the OriginPro 2018 software and Microsoft Excel. The flash-induced fluorescence decay curves and the OJIP transients Chl fluorescence were double normalized; minimal fluorescence F₀ was set to 0 and maximal fluorescence was set to 1. The initial baseline of NADPH and Chl fluorescence curves was shifted to zero.

3 RESULTS

Salt stress has been an important target of research in cyanobacteria and other freshwater microalgae since almost a half-century (Schiewer *et al.*, 1978; Blumwald *et al.*, 1983). However, the exact mechanism of inhibition of different parts of the photosynthetic electron transport pathway has not yet been clarified. To obtain a comprehensive view of the inhibitory sites of salt stress *Synechocystis* cells were exposed to four different concentrations (200, 500, 700 mM, and 1M) of NaCl, and its effect on various sections of the photosynthetic electron transport chain was determined.

3.1 NaCl effect on the oxygen evolution rate

First, we measured the O₂ evolution rate in the absence of an external electron acceptor. In this case, we quantify the activity of the whole electron transport chain, starting from the water-oxidizing complex in PSII, through PSI until CO₂ reduction in CBB cycle. Notably, our observations reveal that in the absence of added electron acceptor higher concentrations of NaCl significantly decreased the capacity of oxygen evolution, which was reduced to ca. 30 % of the untreated control at 1 M NaCl (Figure 1). This observation shows an efficient site of NaCl inhibition somewhere in the whole electron transport chain. Earlier results indicated that one of the inhibitory sites of NaCl could be at the water-oxidizing complex in PSII (Allakhverdiev *et al.*, 2000; Lu & Vonshak, 2002). Therefore, the specific activity of PSII was assessed by measuring the rate of O₂ evolution in the presence of an artificial quinone electron acceptor, DMBQ, which accepts electrons at the Q_B binding site and thus represents the electron transport activity of the PSII complex. The data show that the loss of O₂ evolution rate in the presence of DMBQ relative to the untreated control, also measured in the presence of DMBQ, was much less than in the absence of added acceptor, and ca. 70 % of the original activity was retained even in the presence of 1 M NaCl (Figure 1).

The lower relative inhibition of O₂ evolution in the presence than in the absence of DMBQ shows that the main inhibitory site of NaCl is not in PSII but in the downstream parts of the electron transport process.

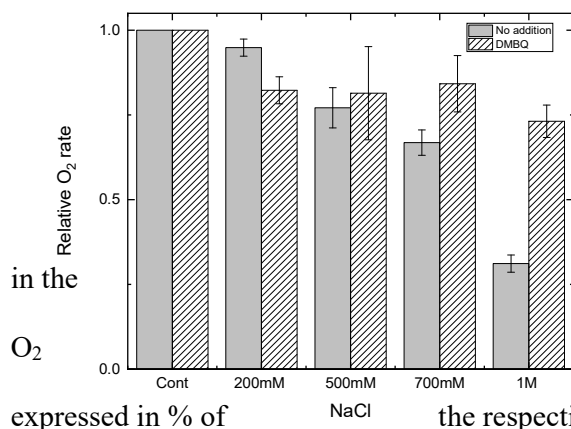


Figure 2 Relative rates of oxygen evolution in the O₂ expressed in % of the respective controls, which were not treated with NaCl. The data represent the mean of three biological replicates with the indicated standard deviation.

3.2 NaCl effect on the OJIP Chl fluorescence transient

To obtain information about the NaCl effect in PSII and its vicinity, including the PQ pool, the so-called OJIP transient of variable Chl fluorescence which reflects linear electron transport through PSII from H₂O to the plastoquinone electron acceptors (Kalaji *et al.*, 2014), was measured (Figure 2). The OJIP transients show a practically unchanged F₀ level, except at 1 M NaCl which induced an F₀ rise (Figure 2A). Normalization of the fluorescence traces to identical F₀ levels reveals a decrease of F_m with increasing NaCl concentrations (Figure 2A inset), showing a decreased capacity of electron transfer from the donor side of PSII to its acceptor side and the PQ pool. Figure 2A also shows an increased J phase with increasing salt concentrations. This effect becomes more clear after double normalization of the fluorescence traces that demonstrates the gradual increase of the J phase, which effect is accompanied by the

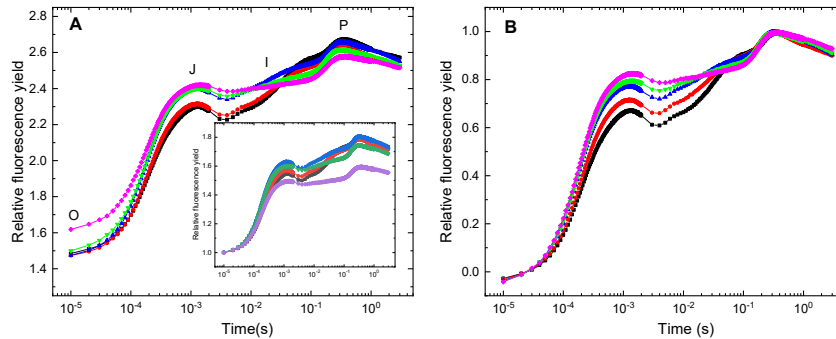
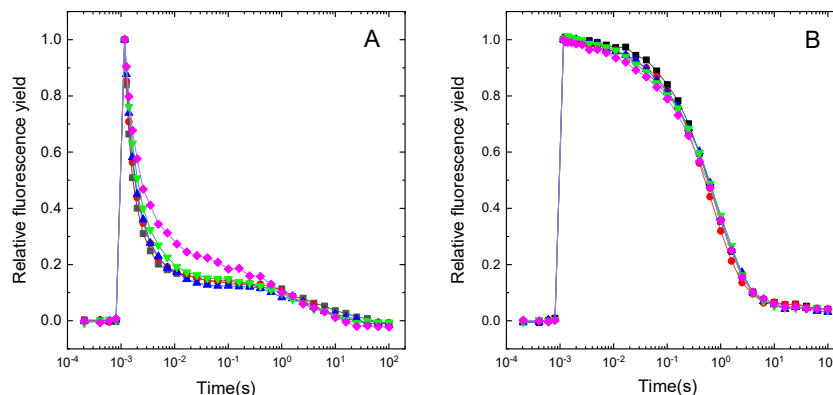


FIGURE 2 Effect of NaCl treatment on the OJIP Chl fluorescence transients in *Synechocystis*. Cells were treated with 0 mM (black), 200 mM (red), 500 mM (blue), 700 mM (green) and 1 M (magenta) NaCl. The fluorescence traces in panel A show representative original traces, the inset shows the same curves after normalization identical F_0 . Panel B shows the curves after double normalization ($F_0=0$ and $F_m=1$). The curves represent the means of 3 biological experiments.

decreased rise of the J-I-P phase (Figure 2B). This observation indicates that electron transport at the acceptor side of PSII is affected by NaCl leading to the accumulation of reduced Q_A , likely to be caused by a decreased efficiency of Q_A^- reoxidation via forward electron transfer. Therefore, our Chl fluorescence transient data indicate that NaCl inhibits both the donor and acceptor sides of PSII, in agreement with previous suggestions (Gong *et al.*, 2008).

3.3 NaCl effect on flash-induced Chl fluorescence relaxation kinetics

To obtain more detailed information on the salt-induced inhibition electron transport at the PSII acceptor side, indicated by the OJIP fluorescence transients, flash-induced Chl fluorescence relaxation measurements were performed (Figure 3). This measurement gives information about the re-oxidation kinetics of Q_A^- via forward electron transfer to Q_B and the PQ pool, and via recombination with donor-side components of PSII. The fluorescence rise after the flash is due to the reduction of Q_A , and the decay observed in the dark is due to the reoxidation of Q_A^- . The relaxation is dominated by the fast phase (300-400 μ s), which reflects electron transfer from Q_A^- to Q_B (or Q_B^-). The middle phase (few ms) arises from the reoxidation of Q_A^- by PQ which



binds to the Q_B site after the flash, whereas the slow phase (few s) arises from the $S_2Q_AQ_B^-$ charge recombination (see (Vass *et al.*, 1999)).

FIGURE 3 NaCl effect on the flash-induced fluorescence relaxation kinetics in *Synechocystis*. Cells were treated with various concentrations of NaCl: 0 mM (black), 200 mM (red), 500 mM (blue), 700 mM (green) and 1 M (magenta). The fluorescence traces in panels A and B show the traces measured in the absence and presence of DCMU, respectively. The traces are shown after normalization to the same initial amplitudes. The actinic flash was fired at the 10^{-3} s time point.

An important effect of NaCl treatment was a slower decay in the fast and middle phases of the signal in the absence of DCMU. In addition, the slow phase of the decay was accelerated (Figure 3A). When the relaxation curves were measured in the presence of DCMU, which blocks the Q_B site and the forward electron transfer from Q_A^- to Q_B a slow decay of the fluorescence yield was observed. The main part of the relaxation has a ca. 0.5 s time constant, which reflects the reoxidation of Q_A^- via charge recombination with the S_2 state of the water-oxidizing complex. NaCl had practically no effect on this decay component. However, with increasing NaCl concentrations a faster (few ms) decay phase also appeared, which is related to the recombination of Q_A^- with a less stable electron donor than the S_2 state, most likely $Tyr-Z^+$ which acts as an electron transport intermediate between the WOC and P680.

Analysis of the decay curves shows that in the absence of DCMU the time constant of the fast phase, which reflects forward electron transfer from Q_A^- to Q_B , increased from ca. 300 μ s (in the untreated control) to ca. 550 μ s in the presence of 1 M NaCl concomitant with the decrease of its relative amplitude from 70 to 60 % (Table 1). The middle phase, which reflects PQ binding to the empty Q_B sites after the flash was also slowed down from 2.4 to 6.2 ms, concomitant with the increase of its amplitude from 21 to 26 % (Table 1), indicating a decrease in the amount of oxidized PQ molecules that could bind to the Q_B site. The slow phase of the decay, which arises from the reoxidation of Q_A^- via charge recombination of the reduced quinone electron acceptor complex ($Q_AQ_B^-$) state with the S_2 state of the water-oxidizing complex, was accelerated with increasing NaCl concentrations from 7.1 s, in the untreated control, to 1.7 s in the 1M NaCl-treated samples (Table 1), which shows the acceleration of the charge recombination from the Q_B^- (via Q_A) with the S_2 state.

NaCl (mM)	Fast phase		Middle phase		Slow phase	
	Amp (%)	t(μ s/ms)	Amp (%)	t(ms)	Amp (%)	t(s)
No addition						
0	70 \pm 2.2	341 \pm 53	21 \pm 2.3	2.4 \pm 0.9	9 \pm 1.1	8.1 \pm 2.4
200	66 \pm 2.4	382 \pm 41	24 \pm 0.9	2.9 \pm 0.4	10 \pm 1.9	5.0 \pm 0.9
500	65 \pm 3.5	492 \pm 74	26 \pm 4.5	4.2 \pm 0.7	9 \pm 1.8	4.1 \pm 2.3
700	60 \pm 5.8	521 \pm 62	30 \pm 7.0	4.6 \pm 0.4	10 \pm 2.5	3.0 \pm 1.6
1000	59 \pm 4.4	551 \pm 30	26 \pm 4.6	6.2 \pm 0.3	15 \pm 4.5	1.8 \pm 0.5
DCMU						
0	4 \pm 3.0	1,48 \pm 1.3			96 \pm 3,0	0.58 \pm 0.07
200	3 \pm 2.2	1.93 \pm 1.2			97 \pm 2.2	0.53 \pm 0.07
500	5 \pm 3.3	7.40 \pm 6.1			95 \pm 3.3	0.58 \pm 0.08
700	7 \pm 3.3	8.95 \pm 7.1			93 \pm 3.3	0.62 \pm 0.07
1000	7 \pm 3.7	6.70 \pm 5.1			93 \pm 3.7	0.58 \pm 0.09

TABLE 1 NaCl effect on the components of the flash-induced Chl fluorescence relaxation

In the presence of DCMU, the main decay phase was in the range of 0.5-0.6 s, without any significant effect by NaCl. However, the amplitude of this slow phase gradually decreased from 99 % (in the untreated control) to 93% in the presence of 1 M NaCl. This effect was accompanied by the increase of a fast phase (few ms) from 1% to 7%. These data are in agreement with the earlier results of (Gong *et al.*, 2008), and also with the slow-down of fluorescence relaxation in the absence of DCMU observed in salt-stressed (150 mM) leaves of fenugreek (*Trigonella foenum graecum*) (Zaghdoudi *et al.*, 2011).

3.4 NaCl effect on flash-induced Chl fluorescence relaxation kinetics under microaerobic conditions

The relaxation kinetics of flash-induced Chl fluorescence can also provide important information about the activity of electron flow into the PQ pool from stromal components. When measured under microaerobic conditions the fluorescence relaxation kinetics show a wave phenomenon, which reflects electron inflow into the PQ pool, mediated by the NDH1 complex in cyanobacteria (Deák *et al.*, 2014) and NDH2 in eukaryotic algae (Krishna *et al.*, 2019; Aslam *et al.*, 2022; Patil *et al.*, 2022). Under microaerobic conditions, the F_0 level rises significantly due to the reduction of the PQ pool, which reduces partly Q_A even in the dark (Figure 4A). After a single-turnover flash PSI-mediated electron transport is oxidizing the PQ pool, resulting in the down-going dip phase reaching its minimal value at around 100 ms, followed by the backflow of the electrons into the PQ pool from the stromal components via NDH-1 (in cyanobacteria (Deák *et al.*, 2014)), or NDH-2 in (eukaryotic algae, (Krishna *et al.*, 2019; Patil *et al.*, 2022)) resulting in the rise (bump) phase of the wave reaching maximal value at around 1s (Figure 4A). NaCl treatment of the cells enhanced the size of the wave (Figure 4B). The deeper dip is consistent with enhanced activity of PSI to oxidize the PQ pool, while the increased bump shows an enhanced inflow of electrons from stromal components.

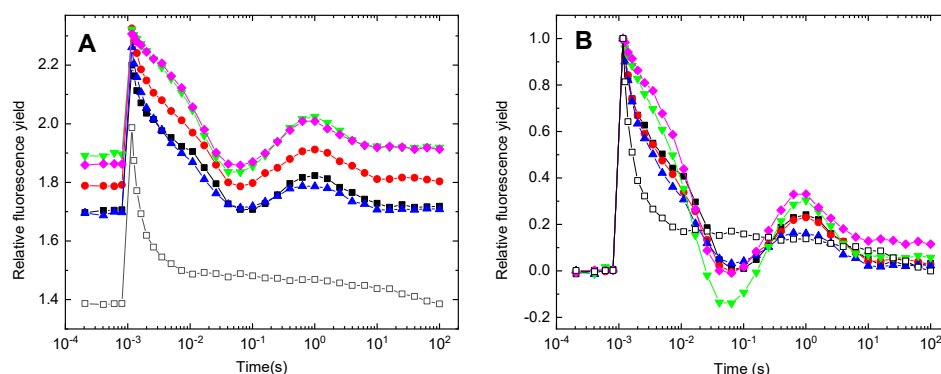


FIGURE 4 NaCl effect on the flash-induced fluorescence relaxation kinetics in *Synechocystis* under micro-aerobic conditions. Cells were treated with various concentrations of NaCl: 0 mM (black), 200 mM (red), 500 mM (blue), 700 mM (green) and 1 M (magenta). The fluorescence traces in panel A show the original representative traces, while in panel B

the same traces are shown after normalization to the same initial amplitudes. The actinic flash was fired at the 10^{-3} s time point.

3.5 NaCl effect on thermoluminescence characteristics

Thermoluminescence is another useful method to obtain information about electron transport processes in PSII, especially on charge recombination between donor and acceptor side components. The two main TL components are the so-called B and Q bands, which arise after excitation with a single-turnover flash from the radiative recombination of the $S_2Q_B^-$ and $S_2Q_A^-$ charge pairs, respectively. Salt treatment induced a decrease in the amplitude of both the B and Q bands (Fig.5). However, the amplitude loss of the B band was significantly larger than that of the Q band. This effect indicates that the stability of reduced Q_B is decreased. Besides the loss of TL intensity there are also characteristics changes in the peak positions. The position of the B band was shifted to lower temperatures in the NaCl-treated samples, and a shoulder also appeared in the position of the Q band, which indicates the partial accumulation of Q_A^- even in the absence of DCMU (Figure 5A). The position of the Q band was slightly upshifted at higher concentrations of NaCl (Figure 5B).

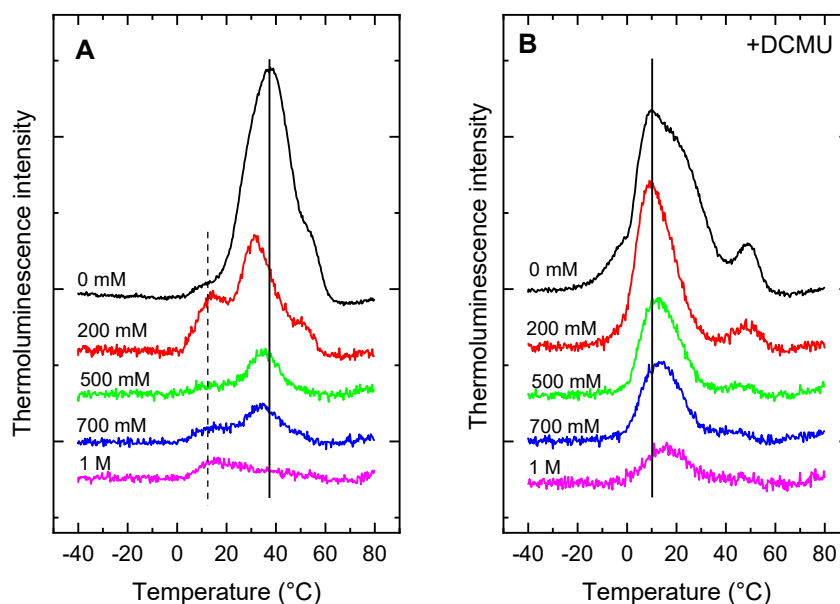


FIGURE 5 NaCl effect on the thermoluminescence characteristics of *Synechocystis*. Cells were treated with various concentrations of NaCl: 0 mM (black), 200 mM (red), 500 mM (blue), 700 mM (green) and 1 M (magenta). Samples shown in panel B were also treated with 10 μ M DCMU. Thermoluminescence was excited by a single turnover saturating flash at -10°C. Samples were quickly cooled to -40°C, to stabilize the charge-separated states and then the luminescence intensity was detected during slow warming (0.5 C/s) in the dark. The plotted curves represent the average of 3-4 biological replicates.

3.6 NaCl effect on the electron transport rate through PSII and PSI

A further approach to analyze the effect of increased NaCl concentrations on photosynthetic electron transport is the measurement of electron transport rates through PSII (ETR(II)) and PSI (ETR(I)) at different light intensities. With the ETR(II) light curve we measure the light intensity dependency of the electron transport rate through PSII, from the water oxidizing complex to the PQ pool, and with ETR(I) the electron transport rate through PSI, from plastocyanin to the PSI acceptor side. ETR(I) is typically larger than ETR(II) since part of the electrons passing through PSI are cycled back to the PQ pool and the donor side of PSI. This effect is present in the untreated control, but enhanced in the presence of NaCl (Figure 6 A, D, G, J). With increasing NaCl

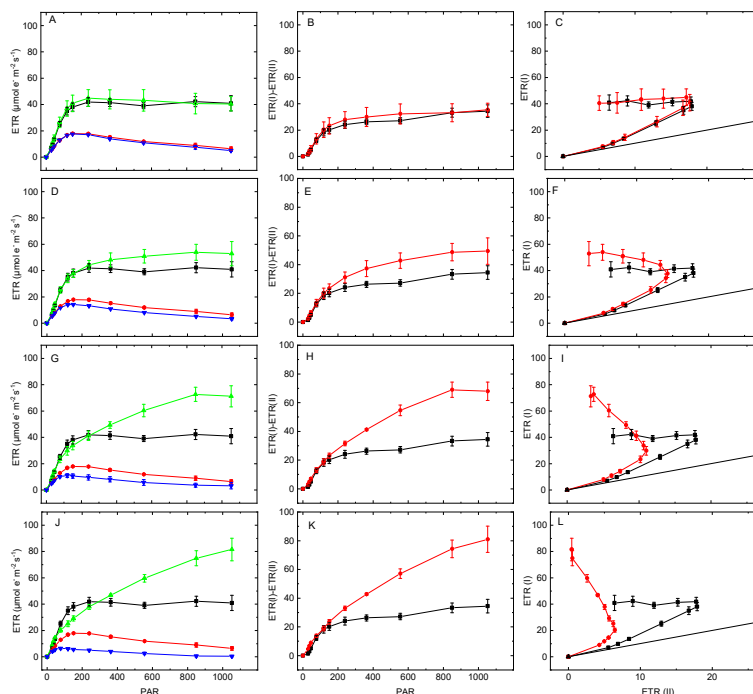


FIGURE 6 NaCl effect on the PSII and PSI electron transport rates in *Synechocystis*. Cells were treated with various concentrations of NaCl (200 mM (A), 500 mM (D), 700 mM (G), 1 M (J)) and the ETR(II) (blue and red curves), and ETR(I) (black and green curves) electron transport rates were measured as a function of light intensity. The black and red curves in Panels A, D, G, and J show ETR(I) and ETR(II) of the untreated control, respectively. In panels B, E, H, K the difference of ETR(I) – ETR(II) is shown for 200, 500, 700 mM, and 1 M NaCl (red curves), as well as for the untreated control (black curves), respectively. In panels C, F, I, L the ETR(I) values are shown as a function of ETR(II) for the 200, 500, 700 mM, and 1 M NaCl-treated cells (red curves), as well as for the untreated control (black curves), respectively. The straight black line shows the ideal case for a linear relationship between ETR(I) and ETR(II). The data represent mean values obtained from three independent biological replications with the indicated standard deviations.

ETR(II) is decreased and ETR(I) is increased especially at higher light intensities. This shows that the activity of PSII is inhibited by NaCl, but the activity of PSI is apparently enhanced.

As a consequence, the difference between ETR(I) and ETR(II) is also increased (Figure 6B, E, H, K) indicating enhanced cyclic electron flow above 500 mM NaCl.

An alternative approach to analyze cyclic electron flow is to plot ETR(I) as a function of ETR(II) (Figure 6 C, F, I, L). If there were just linear electron flow through PSII and PSI without branching to a cyclic pathway after PSI, then ETR(I) should be equal to ETR(II) as represented by the straight black line in Figure 6 C, F, I, L). However, the measured data follow this ideal case only in the first few points, i.e. at low ETR values obtained at low light intensities. At higher ETR values the ETR(I) vs. ETR(II) curve deviates towards ETR(I) showing the onset of cyclic electron flow. In the presence of NaCl the deviation from the linear relationship starts at lower ETR values (lower light intensities), and it is enhanced relative to the untreated control (Figure 6 C, F, I, L), showing increased cyclic electron flow in the NaCl treated cells.

3.7 NaCl effect on the electron transport of PSI

The ETR(I) and ETR(II) measurements, described above, indicated that although the overall activity of PSI was affected only to a small extent by NaCl, or even enhanced at higher NaCl concentrations, the ratio of linear and cyclic electron transport pathways was modified. To access this process in more detail the kinetics of $P700^+$ were measured. During the measurement after detecting the dark level of the $P700^+$ signal sub-saturating intensity FR light was applied, which induces charge separation in PSI keeping P700 partly oxidized. The steady-state level of the $P700^+$ signal is determined by the equilibrium of FR-induced oxidation of P700 and re-reduction of $P700^+$ by charge recombination in PSI as well as by the electrons coming from PSII via the $cytb_6f$ complex PC and via cyclic electron flow. Complete oxidation of P700 can be accomplished by a saturating intensity light pulse, which increases $P700^+$ to its maximal level. After switching off the light pulse the $P700^+$ signal decreases below the steady-state level due to the effect of electrons coming from the direction of PSII (Figure 7), and then elevated again due to the oxidizing effect of the far-red light. When the PSII activity is inhibited by DCMU the steady-state level of $P700^+$ increases and the undershoot after the saturating pulse disappears. Both of these effects are due to the lack of electrons arriving from PS II.

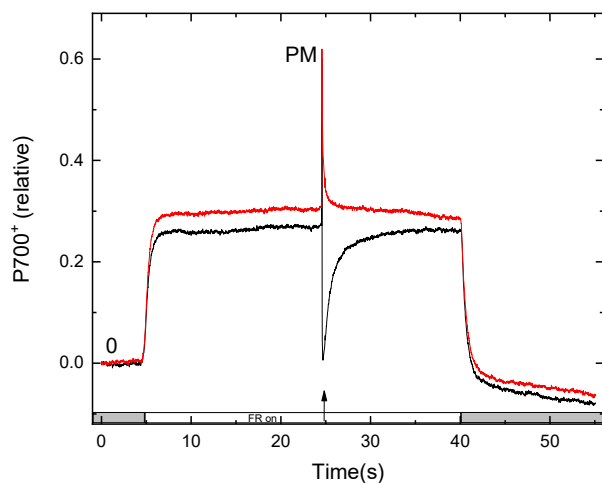


FIGURE 7 Kinetics of P700⁺ formation in *Synechocystis*. The P700⁺ traces were measured without addition (black curve) and in the presence of DCMU (red curve) and shown after double normalization to the dark (0) and Pm levels to achieve the same total amplitudes. The grey bar represents a measurement in the dark and the white bar represents the Far-red illumination, the arrow represents the saturating pulse.

When the cells were exposed to the NaCl treatment, we observed that on the one hand, the undershoot of the P700⁺ signal after the saturating pulse was decreased (Figure 7) indicating that fewer electrons are coming from the direction of PSII due to its salt-induced inhibition. On the other hand, the steady-state level of the signal was also decreased, which shows that in the salt-treated cells, there is a higher overall rate of electrons arriving at the donor side of PSI than in the untreated control. Since NaCl partly inhibits PSII electron transport as shown by the decreased ETR(II) level (Figure 6) and by the decreased undershoot of the P700⁺ signal (Figure 8) the decreased steady-state level can be explained by an enhanced electron flow coming from stromal electron transport components to the PQ pool. Since the net change of the P700⁺ steady-state is a decrease relative to the control (Figure 8), this shows that the enhancement of the cyclic pathway is larger than the decrease of the linear pathway due to NaCl-induced inhibition of PSII.

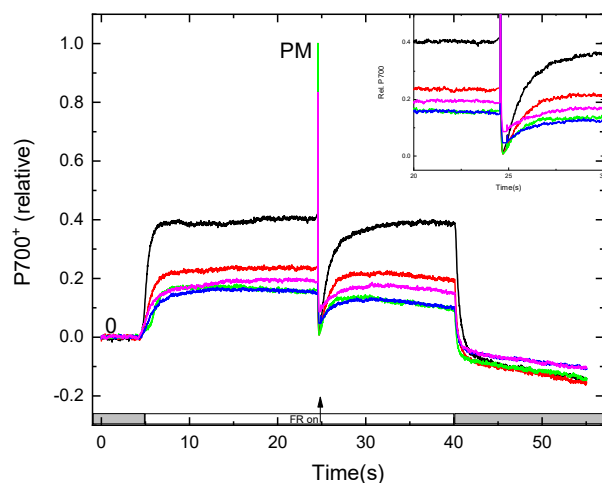


FIGURE 8 NaCl effect on the P700⁺ kinetics *Synechocystis*. The P700⁺ traces were measured without addition (black curve) and in the presence of various concentrations of NaCl (200 mM red, 500 mM cyan, 700 mM green and 1 M blue). The curves are shown after double normalization to the dark (0) and Pm levels to achieve the same total amplitudes. The inset shows the enlarged area of the undershoot following the saturating pulse. (The grey bar represents a measurement in the dark and the white part represents the FR (Far-red) on, the arrow represents the saturating pulse).

3.8 NaCl effect on linear electron transport components downstream of PSI

3.8.1 NaCl effect on NADPH fluorescence kinetics

An important step of linear electron transport is the production of NADPH via electrons coming from the acceptor side of PSI through ferredoxin (Fd) and FNR. To explore

the effect of increased NaCl concentrations on this part of the linear electron transport chain the kinetics of NADPH production were measured by detecting NADPH fluorescence. Light-induced NADPH fluorescence was characterized by dark-light-dark kinetics (Schreiber & Klughammer, 2009). Initial NADPH fluorescence was measured for 30 s in darkness to obtain the steady state level of the NADPH pool in the dark. The initial rise initiated by the onset of actinic illumination ($56 \mu\text{mol photons m}^{-2}\text{s}^{-1}$) is followed by a pronounced dip phase, before a second rise phase sets in where the light driven reduction of NADP pool takes place (Figure 9A). The secondary rise reflects NADPH synthesis from linear electron flow. After reaching a peak level at ca. 20 s a gradual decline of the NADPH level was observed that likely reflects NADPH consumption by activation of CBB cycle for CO_2 fixation. After turning off the actinic light, there was a sharp decline in the NADPH fluorescence reaching its minimum below the dark steady-state level, as linear electron flow ceases to drive electrons into the NADPH pool in the dark, yet NADPH consumption pathways remain in their active state resulting in a dark oxidation of NADPH leading to an undershoot of the NADPH level before it is stabilized again in the dark.

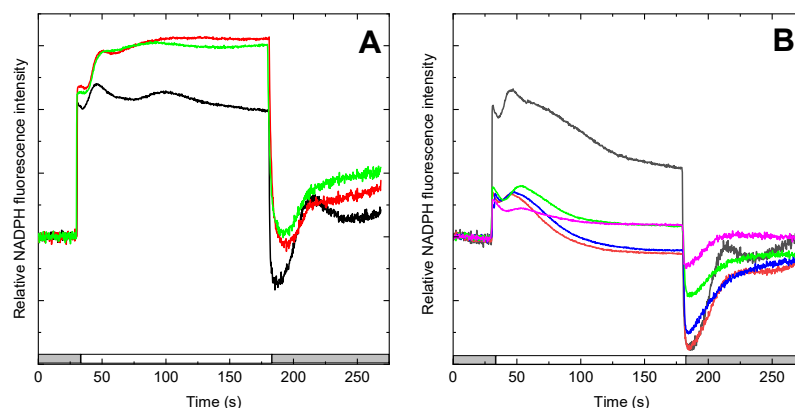


FIGURE 9 Glycolaldehyde and NaCl effect on NADPH fluorescence kinetics in *Synechocystis*. A, cells were treated with 5 mM (red) and 10 mM glycolaldehyde (green) and compared to the untreated control (black). B, Cells were treated with 0 mM (black), 200 mM (red), 500 mM (green), 700 mM (blue), as well as with 1 M (cyan) NaCl. Curves were normalized to the same dark steady-state levels. (The grey bar represents measurement in the dark and the white part represents the actinic light on).

When the CBB cycle was inhibited by the addition of glycol aldehyde (GA) the decline of the NADPH signal after the second rise was eliminated and the signal was stabilized at a high level. This observation confirms that the decline of NADPH after its maximum level in the light is due to its consumption by the CBB cycle. Importantly, the undershoot of the signal below the dark equilibrium level was also eliminated by GA, confirming that this effect is due to the activity of the CBB cycle, which proceeds for a limited period of time in the dark after switching off the light.

Salt treatment decreased the initial rise of NADPH fluorescence after the onset of actinic light, which shows that NaCl reduces the light-dependent production of NADPH via the linear electron transport pathway (Figure 9B). Besides this effect the decline of the signal after the maximal level was decreased in a NaCl-concentration-dependent manner and was almost eliminated at 1 M NaCl (Figure 9B). Furthermore, the undershoot of the signal below

the dark steady-state level was also decreased with increasing salt concentrations and was completely eliminated at 1 M NaCl (Figure 9B). These data strongly indicate that NaCl induces a concentration-dependent inhibition of NADPH consumption, both in light and in darkness, which reaches the level of complete inhibition at 1 M.

3.8.2 NaCl effect on post-illumination chlorophyll fluorescence rise transients

Although Chl fluorescence kinetics are primarily determined by electron transport processes in PSII, i.e. the reduction level of Q_A , downstream effects as far as NADPH consumption and re-production in the CBB cycle can also be detected by slow kinetic changes of Chl fluorescence (Kalaji *et al.*, 2014) recorded in parallel with the NADPH kinetics as shown in Figure 10. The first 30 s of the curve is recorded in dark with weak measuring light to determine the minimum fluorescence (F_0) level. After switching on the actinic light, an increase in Chl fluorescence can be observed (Figure 10A), whose kinetics in general indicate the progressive increase in the number of closed PSII reaction centers reported by the accumulation of reduced Q_A . This reflects a quasi-steady state balance of rates corresponding to the actinic excitation rate generating Q_A^- (Q_A reduction rate) and the rate of forward electron transfer of electron into the PQ pool via the PSII Q_B site (Q_A^- re-oxidation rate). After switching off the light the fluorescence level drops close to F_0 , but after that shows a slow rise in the few tens of seconds timescale, which effect is termed as post-illumination fluorescence rise. This effect is assigned to the reversal of the CBB cycle in the dark during which NADPH is re-formed at the expense of the Calvin cycle intermediate DHAP (Mano *et al.*, 1995; Gotoh *et al.*, 2010) and the electrons from NADPH are transferred back the PQ pool, and finally to Q_A , which results in the fluorescence rise. In our samples, the post-illumination fluorescence rise transient appeared ca. 40-50 s after switching off the actinic light (Figure 10A).

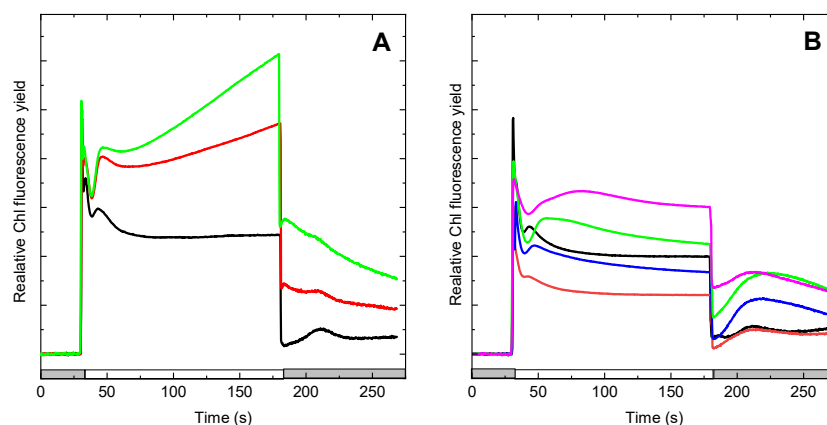


FIGURE 10 Effect of glycolaldehyde and NaCl on the slow Chl fluorescence induction kinetics in *Synechocystis*. A, Cells were either left untreated (black), or treated with 5 mM (red) or 10 mM (green) GA. B, Cells were treated with NaCl at 0 mM (black), 200 mM (red), 500 mM (green), 700 mM (blue), or 1 M (cyan).

One of the characteristic effects of NaCl treatment on the slow Chl fluorescence transient was the increase of the steady-state level at higher NaCl concentrations (Figure 10B), which was also observed in the presence of GA (Figure 10A). The other interesting effect was the enhancement of the post-illumination rise transient, which was the most

pronounced at 0.5 M NaCl, but then gradually decreased at higher concentrations. The phenomenon of post-illumination fluorescence rise arises from the reduction of the PQ pool by the electrons from photoreductants accumulated during partial reversion of the CBB cycle (Gotoh *et al.*, 2010). This idea is supported by the suppression of the transient in the presence of the CBB cycle inhibitor GA (Figure 10A), which acts at the level phosphoribulokinase (PRK) (Miller & Calvin, 1989). The enhancement of the post-illumination rise transient indicates that NaCl has multiple action sites in the CBB cycle as discussed in detail below.

4 DISCUSSION

The inhibitory effects of salt stress on the process of photosynthetic electron transport have been studied for several decades. However, no consensus picture has been established yet concerning the identity of the inhibitory sites and their relative importance. The main points of contradiction concern the inhibitory sites in PSII, the effect of salt on PSI activity, as well as inhibitory sites downstream of PSI, with special emphasis on the activity of the CBB cycle.

4.1 Salt-induced inhibition of PSII

4.1.1 Salt-induced effects on the donor side of PSII

There is a consensus that NaCl in 0.2-0.8 M inhibits the activity of PSII, as reported in the early salt stress studies in *Synechocystis* by (Schubert & Hagemann, 1990). However, the suggested site(s) of salt-induced inhibition within PSII are partly contradictory (for reviews see (Sudhir & Murthy, 2004; Allakhverdiev & Murata, 2008; Yang *et al.*, 2020; Pan *et al.*, 2021).

Lu and Vonshak (Lu & Vonshak, 1999) found in *Spirulina platensis* that electron transport from H₂O to MV, DPC to MV, and H₂O to pBQ was inhibited to identical extents and it was concluded from these results that salt stress inhibits the PSII reaction center rather than the oxidizing or reducing side of PSII. Allahverdiev and Murata (Allahverdiev *et al.*, 1999; Allahverdiev *et al.*, 2000) reported that 0.5 mM NaCl inhibited PSII activity in *Synechococcus* PCC 7942. In contrast to Lu and Vonshak, they concluded that this effect was not related to decreased activity of the PSII reaction center (including P680, Phe, and Q_A), and only the electron transport from the WOC to the RC was blocked. Later works supported the idea that the water-oxidizing complex (WOC) of PSII is an actual site of salt-induced inhibition (Lu & Vonshak, 2002). Based on variable Chl (Chl) and thermoluminescence measurements it was suggested that the inhibition of PSII donor side activity is possibly related to the destabilization of the catalytic Mn complex due to salt-induced release of the Mn-stabilizing PSBO protein (Gong *et al.*, 2008).

Our data showing decreased O₂ evolution in NaCl-treated *Synechocystis* cells in the presence of an artificial quinone electron acceptor DMBQ, that accepts electrons from PSII, (Figure 1) confirms NaCl-induced inhibition of PSII. On the other hand, the NaCl-induced retardation of Chl fluorescence rise in the so-called OJIP transient, resulting in a decreased F_m level (Figure 2A inset), demonstrates that the capacity of PSII to deliver electrons from its WOC to the acceptor side of PSII is decreased by salt stress, and thus confirms an inhibitory site of NaCl at the PSII donor side in the WOC.

4.1.2 Salt-induced effects on the acceptor side of PSII

Although results from early works were interpreted as showing that salt stress had no effect on the acceptor side electron transport of PSII (Lu and Vonschak, 1999) subsequent studies indicated an acceptor side limitation in *Spirulina platensis*, which was assigned to an increased proportion of Q_B-nonreducing centres resulting in the accumulation of reduced Q_A (Lu & Zhang, 1999). In later works it was found that salt stress (up to 0.8 M NaCl) affects the PSII acceptor side, results in the accumulation of Q_A⁻ due to inhibited electron transfer from Q_A⁻ to Q_B (Lu & Vonschak, 2002). The inhibited Q_A⁻ to Q_B electron transfer was confirmed by a follow-up work in *Spirulina platensis* by (Gong *et al.*, 2008) using flash-induced Chl fluorescence relaxation kinetic measurements, and also in *Microcystis* ssp. (Dabrowski *et al.*, 2021). In a related context (Zaghdoudi *et al.*, 2011) observed that the flash-induced fluorescence decay kinetics were progressively slower as salt stress increased (150 mM NaCl) in the leaves of fenugreek (*Trigonella foenum graecum*). It was also suggested that NaCl induced a redox potential decrease of the Q_B/Q_B⁻ redox pair *Spirulina platensis* (Gong *et al.*, 2008).

Our results with the relaxation of flash-induced Chl fluorescence yield fully confirm the inhibitory effect of NaCl at the acceptor side of PSII leading to a concentration-dependent inhibition of the Q_A⁻ to Q_B electron transfer (Figure 3A). Analysis of the fluorescence relaxation curves presented in Table 1. showed the slow-down of the fast phase (from ca. 300 μs to 500 μs), which reflects Q_A⁻ reoxidation by PQ (Q_B) bound to the Q_B site at the time of the flash. The middle phase of the relaxation, which arises from the reoxidation Q_A⁻ by a PQ that binds to the Q_B site after the flash, was also slowed down (from ca. 3 ms to 6 ms). Interestingly, the slow phase of the fluorescence relaxation, which arises from the charge recombination of Q_B⁻ (via charge equilibrium between Q_A⁻Q_B and Q_AQ_B⁻) with the S₂ state of WOC was accelerated (from ca. 7s to 1.8 s) with a concomitant increase of its amplitude (from 8 to 11%). In the presence of DCMU which blocks the Q_B site, the main phase of the relaxation reflects the recombination of Q_A⁻ with the S₂ state, its time constant is ca. 0.5s and practically independent from the presence of NaCl. In the presence of DCMU there is also a small fast phase, with ca. 1-2 ms time constant and a few % relative amplitude (Table 1.) This phase can be assigned to the recombination of Q_A⁻ with a PSII donor side component, which is energetically less stable than the S₂ state. Previous data with PSII donor side mutants indicate that this component is likely Tyr-Z⁺. The salt-induced increase of the relative amplitude of the fast phase in the presence of DCMU is consistent with the inhibition of the WOC, which in the inhibited state cannot accumulate positive charges in the S-states and therefore cannot act as a recombination partner.

The acceleration of the charge recombination kinetics in the absence (S₂Q_AQ_B⁻), but not in the presence of DCMU (S₂Q_ADCMU) shows that the energetic stability of the Q_B/Q_B⁻ redox pair is decreased relative to that of Q_A/Q_A⁻. According to previous results about the functioning of the Q_AQ_B acceptor complex, the equilibrium constant of sharing the electron between the Q_A⁻Q_B and Q_AQ_B⁻ states can be obtained from the ratio of the recombination time constants $K_{app} = t_{S_2Q_B} / t_{S_2Q_A} - 1$ (Robinson & Crofts, 1983; Diner *et al.*, 2001). On the other hand, the charge equilibrium is a thermally activated process, with $K_{app} = \exp(\Delta G/kT)$, where ΔG is the free energy (redox) gap between Q_B/Q_B⁻ and Q_A/Q_A⁻, k is the Boltzmann's constant, T is the absolute temperature. From these expressions, the ΔEm(Q_B/Q_B⁻ - Q_A/Q_A⁻) redox gap (whose value in mV units is numerically the same as of the ΔG free energy gap in meV) can be obtained as $\Delta E_m = k * T * \ln(K_{app})$. By using the data in Table 1. we obtain $K_{app} = 13$ and 66 mV redox gap between ΔEm(Q_B/Q_B⁻ - Q_A/Q_A⁻) in agreement with previous reports (Robinson & Crofts, 1983; Demeter *et al.*, 1985; Gong *et al.*, 2008). In NaCl-treated cells, K_{app} was decreased with increasing NaCl concentrations (8.4, 6.1, 3.8, and 2.1 at 200 mM, 500 mM, 700 mM, and 1M, respectively) resulting in the decrease of the redox gap to 19 mV in 1M

NaCl-treated samples. These data are in good agreement with previous results obtained in *Spirulina platensis* (Gong *et al.*, 2008) and confirm that in contrast to the suggestion of Murata and coworkers NaCl induces inhibition of PSII electron transfer not only in the WOC at the PSII donor side but also at the PSII acceptor side at the level of the Q_A^- to Q_B electron transfer step.

In the interesting work of Gong *et al.* (Gong *et al.*, 2008) whose main conclusions are supported by our results, the authors suggested that salt-induced release of the 33 kDa Mn-stabilizing PsbO protein could be responsible for both the inactivation of the WOC, and also for the destabilization of Q_B/Q_B^- due to a conformational change which is transmitted from the donor side of PSII to its acceptor side. However, previous results obtained with a PsbO deletion mutant in *Synechocystis* 6803 showed that the absence of PsbO increases preferentially the energetic stability of Q_A/Q_A^- , showing a 12 °C upshift of the peak position of the Q TL band, and leaves Q_B/Q_B^- practically unaffected, shown by a ca. 5 °C downshift in the peak position of the B band (Vass *et al.*, 1992). Similar results were obtained in isolated PSII membrane particles where the Q band was upshifted by 20 °C after removal of the 16, 23, and 33 kDa (PsbO) peripheral proteins by $CaCl_2$ or urea+NaCl washing, while NaCl washing alone, which removes only the 16 and 23 kDa proteins did not affect the peak position of the Q band, but decreased the peak position of the B band by 5C (Vass *et al.*, 1987).

Our TL data indicated only a minor upshift of the Q band (Figure 5), which could be due to the presence of a small TL component at the high-temperature side of the curve, which becomes visible when the intensity of the main band is decreased (see (Vass *et al.*, 1981). This idea is confirmed by the observation that the flash fluorescence decay time arising from $S_2Q_A^-$ in the presence of DCMU was not increased by the NaCl treatment neither in our study (Table 1), nor in the study of Gong *et al.* (Gong *et al.*, 2008) showing that the energetic stability of the $S_2Q_A^-$ charge pair was not affected by the NaCl treatment.

Therefore, we do not think that NaCl-induced removal of PsbO could be the main cause for the inhibition of the PSII donor and acceptor side electron transport. On the other hand, the in vitro NaCl treatment data indicated that NaCl washing of PSII particles, which removed the 16 and 23 kDa peripheral proteins from the PSII donor side but left PsbO bound to PSII, induced a decrease in the peak position of the B thermoluminescence band, but had no effect on the peak temperature of the Q band (Vass *et al.*, 1987). Since the Q and B bands arise from the $S_2Q_A^-$ and $S_2Q_B^-$ charge recombination, respectively, the downshifted B band together with the unchanged Q band indicates a destabilization of Q_B/Q_B^- just as our flash fluorescence data show. The larger extent of the decrease of the B band intensity compared to that of the Q band indicates that the binding stability of Q_B^- in the Q_B binding site is also decreased in the NaCl-treated cells.

It is also of note that the loss of the intensity of the TL B and Q bands in the NaCl-treated cells (Figure 5) is much larger than that would be expected from the decrease of the O_2 evolution rate in the presence of DMBQ (Figure 1). This apparent discrepancy is most likely caused by the different measuring conditions, i.e. a single-flash excitation of the TL followed by a long, tens of seconds period in the dark during warming up the samples, versus a strong continuous illumination during the O_2 evolution measurements. The loss of TL intensity indicates that the positive charge stored in the S2 state can be lost in a relatively slow process during the TL measurement due to an effect of cellular reductants that can have access to the WOC after disturbing the integrity of the PSII donor side by the NaCl treatment. In contrast, the rapid turnover of the S-state cycle at high light intensity during the O_2 evolution measurement can compensate for the slow destabilization of the S2 state.

Based on our data, we prefer the idea that the NaCl-induced modifications of the PSII donor and acceptor side electron transport processes are likely to be related to the NaCl-

induced modification of the integrity of the PSII structure which leads to decreased stability of charge storage both in the S₂ state and Q_B⁻. Our data do not support that a preferential release of the PsbO protein would be responsible for this effect but may be related to the removal of the 16 and 23 kDa proteins.

4.2 Salt-induced effects on PSI activity

The effect of salt stress on Photosystem I, the other main membrane-bound component of the electron transport chain, is also contradictory. On the one hand PSI activity from reduced DCPIP acting as an electron donor directly to PSI, to the MV electron acceptor at the acceptor side of PSI, was found to be significantly enhanced (to 180% of the untreated control) in *Spirulina platensis* (Lu & Vonshak, 1999) in agreement with earlier findings by (Joset *et al.*, 1996). The enhanced PSI activity in salt-treated *Spirulina platensis* cells was later confirmed by (Sudhir & Murthy, 2004; Sudhir *et al.*, 2005) and also by Zhang *et al.* (Zhang *et al.*, 2010). However, Allakhverdiev and Murata observed a ca. 50% loss of PSI activity in the presence of 0.5 M NaCl, by measuring O₂ uptake from DCIP to MV (Allakhverdiev & Murata, 2008), which is in strong contrast with the substantial PSI activity increase described above. To address this question we measured light intensity dependence of electron transport rates through PSI (ETR(I)) and PSII (ETR(II)), as well as the oxidation-reduction kinetics of P700.

Our data, presented in Figure 6, fully support the earlier findings which show enhanced PSI activity in NaCl-treated *Synechocystis* (and other cyanobacterial) cells and are in clear contrast with the results suggesting almost the same inhibition of PSI as of PSII (Allakhverdiev & Murata, 2008). Larger ETR(I) than ETR(II) indicates enhanced cyclic electron flow around PSI. This can be represented by the difference between the ETR(I) and ETR(II) values, which shows that the rate of cyclic electron flow is gradually enhanced with increasing NaCl concentrations (Figure 6 B, E, H, K). Another representation of the presence of cyclic flow is the plotting of ETR(I) as a function of ETR(II), where the upward deviation of ETR(I) from the linear relationship shows the passing of electrons through PSI which do not originate from PSII. This NaCl-induced enhancement of cyclic electron flow confirms earlier results, see (Sudhir & Murthy, 2004).

Besides measuring ETR(I) we used another approach to characterize PSI activity in NaCl-treated cells. This approach is based on the oxidation of P700 by using non-saturating FR light in combination with a saturation white light pulse (that saturates both PSI and PSII) (Szabo *et al.*, 2017). The steady-state level of P700⁺ is determined by the balance of the non-saturating FR light, that oxidizes P700, and the electron flow to the donor side of PSI from PSII (which is also driven partly by FR light) and from the cyclic pathways. Application of a short saturating white flash induces the maximal oxidation of P700, followed by a transient decrease of the P700⁺ level below the steady state due to re-reduction of P700⁺ by electrons arriving from PSII. This idea is confirmed by the application of DCMU to block PSII electron transfer, which increases the steady-state P700⁺ level in FR light and eliminates the undershoot of the P700⁺ signal during the saturating pulse (due to inhibited electron flow from PSII).

The decrease of the undershoot during the saturating pulse by increasing NaCl concentrations (Figure 8) confirms the inhibition of PSII-derived electron flow towards PSI. Interestingly, the steady state level of P700⁺ was also decreased in the NaCl-treated cells, which shows that although the electron transport rate from the direction of PSII was decreased the total electron transport rate that reaches the donor side of PSI, i.e. 700⁺, increases. This effect can be explained by NaCl-induced enhancement of electron flow via the cyclic and alternative (stromal origin) pathways. The enhanced formation of the wave phenomenon in

the relaxation kinetics of flash-induced Chl fluorescence (Figure 4) indicates that the enhanced electron flow is mediated partly by the NDH1 complex, which is responsible for the fluorescence wave in cyanobacteria (Deák *et al.*, 2014). The origin of these electrons arriving from stromal components via NDH1 can be either respiration, which is known to be enhanced by NaCl treatment (Jeanjean *et al.*, 1993; Zeng & Vonshak, 1998), or the NaCl-induced inhibition of the CBB cycle (discussed below) which eliminates a major NADPH sink and therefore increases the stromal concentration of NADPH.

4.3 Salt-induced effects on electron transport components downstream of PSI

The measurements of oxygen evolution rates showed that NaCl-induced inhibition of the linear electron transport was much larger in the absence of added electron acceptor, i.e. when CO₂ acted as the final electron acceptor in the CBB cycle, than in the presence of DMBQ accepting electrons directly from PSII (Figure 1). These data together with the finding that PSI activity was not reduced, but rather enhanced, by NaCl treatment show that the main inhibitory site of NaCl is somewhere downstream of PSI.

Measurements of NADPH kinetics during light-to-dark and then dark-to-light transitions showed three notable effects. One of them is the decreased amplitude of NADPH production after switching on the light (Figure 9B), which can be explained by the reduced capacity of PSII to deliver electrons for linear electron transport. However, the NaCl also inhibited the decline of NADPH after its transient maximum in the light and the undershoot of the signal below the initial dark level after the light-to-dark transition. The decline of the NADPH level in the light after reaching its maximum reflects NADPH consumption by the CBB cycle in the light, whereas the rapid decrease of NADPH after switching off the light to a level lower than the initial dark level is due to the oxidation of the NADPH pool by glyceraldehyde 3-phosphate dehydrogenase in the CBB cycle which goes in for some time in the dark (Kauny & Setif, 2014; Kusama *et al.*, 2022). In agreement with this explanation, the inhibited decline of NADPH in the light and also of the undershoot after the light-to-dark transition was also observed when the CBB cycle was inhibited by glycol aldehyde (GA) (Figure 9A), which blocks the cycle at the level of phosphoribulokinase (PRK) (Miller & Calvin, 1989). Based on the comparison with the GA effect we conclude that NaCl inhibits the CBB cycle activity above 500 mM.

To identify the site(s) of NaCl-induced inhibition within the CBB cycle we utilized the kinetic changes of variable Chl fluorescence measured in parallel with NADPH fluorescence. A characteristic feature of the Chl fluorescence transients is the so-called post-illumination fluorescence rise, which is the transient increase of the fluorescence yield following the light-to-dark transition in the tens of seconds time range (Figure 10). Post-illumination increase in Chl fluorescence has been found in C4 (Asada *et al.*, 1993) and C3 plants (Mano *et al.*, 1995), and cyanobacteria (Mi *et al.*, 1995). The phenomenon was explained as the reduction of plastoquinone (PQ) by the electrons from photoreductants accumulated in the stroma or cytosol during illumination and may reflect cyclic electron transport around PSI mediated by NDH-1 in cyanobacteria (Mi *et al.*, 1995) and by plastid NADH dehydrogenase-like complex in higher plants (Shikanai *et al.*, 1998). The appearance of the post-illumination fluorescence transient was assigned to the accumulation of the CBB cycle intermediate dihydroxyacetone phosphate (DHAP) in *Arabidopsis* (Gotoh *et al.*, 2010) from which reverse electron flow via NADPH and the NDH complex delivers electrons to the PQ pool. It was also shown that the inhibition of fructose-1,6-bisphosphate aldolase (FBA) induces the post-illumination rise transient by inhibiting the conversion of DHAP to fructose-1,6-bisphosphate (FBP) (Gotoh *et al.*, 2010). The process is most likely via the same pathway in cyanobacteria, therefore we can conclude that one of the NaCl inhibitory sites in the CBB cycle, which is responsible for the

increase of the post-illumination fluorescence rise transient up 500 mM, is located after DHAP formation, perhaps at fructose-1,6-bisphosphate aldolase (FBA). The decrease of the post-illumination fluorescence transient at higher than 500 mM NaCl can be explained by a second, lower affinity inhibitory site which inhibits the NADPH requiring DHAP formation (Mano *et al.*, 1995; Gotoh *et al.*, 2010), perhaps at the same place (PRK) where GA acts.

In higher plants, salt-induced inhibition of CO₂ uptake by the CBB cycle is usually assigned to the inhibition of the photosynthetic activity of guard cells of stomata by NaCl. However, besides stomatal limitation, NaCl stress seems to inhibit directly the activity of several enzymes of the CBB cycle, especially Rubisco, fructose-1,6-bisphosphatase (FBPase), fructose-1,6-bisphosphatase aldolase (FBPA), and PRK (Yang *et al.*, 2008; Pan *et al.*, 2021). These data support our assignment of direct NaCl inhibitory sites in the CBB cycle.

5 CONCLUSIONS

The impact of salt stress on the photosynthetic processes was investigated in the model cyanobacterium *Synechocystis* 6803 to resolve long-standing contradictions in the literature regarding the sites of NaCl-induced inhibition at the donor and acceptor sides of PSII, and of PSI, as well as to explore the inhibitory effects of salt stress downstream of PSI. Our data confirm that NaCl inhibits both the water-oxidizing complex at the donor side of PSII, as well as the functioning of the Q_AQ_B two-electron gate at the acceptor side of PSII. We also demonstrated that the preferential NaCl effect on the PSII acceptor side is at Q_B by inducing the decrease of the binding stability of Q_B⁻ and of the energetic stability of the Q_B/Q_B⁻ redox pair. Our data also confirmed that the rate of electron transport through PSI is not inhibited, but enhanced in NaCl-treated cells, due to enhanced electron flow into the PQ pool via cyclic and NDH1-mediated pathways from stromal sources.

Our data demonstrated that the main inhibitory sites of salt stress are located downstream of PSI. In the CBB cycle we identified two inhibitory sites of NaCl: One site, with higher affinity, is located after DHAP formation, possibly at fructose-1,6-bisphosphate aldolase. A lower affinity site is located before DHAP formation, perhaps at PRK or Rubisco.

Competing interests

None declared

Author contributions

IV conceived the idea and conceptualized the study. PPP, SK, and MSZ performed the experiments. PPP prepared the figures and wrote the first draft of the paper, IV finalized the conclusions and the text of the paper. All the authors approved the final version of the manuscript.

Funding: This research was funded by the National Research, Development, and Innovation Office, grant number K-132568

ORCID

Imre Vass, <https://orcid.org/0000-0003-4987-7842>

Data availability

The data that support the findings of this study are all presented in the figures and tables.

REFERENCES

- Allakhverdiev SI, Murata N. 2008.** Salt stress inhibits photosystems II and I in cyanobacteria. *Photosynthesis Research* **98**(1-3): 529-539.
- Allakhverdiev SI, Nishijama Y, Suzuki I, Tasaka Y, Murata N. 1999.** Genetic engineering of the unsaturation of fatty acids in membrane lipids alters the tolerance of *Synechocystis* to salt stress. *Proc. Natl. Acad. Sci. USA* **96**: 5862-5867.
- Allakhverdiev SI, Sakamoto A, Nishiyama Y, Inaba M, Murata N. 2000.** Ionic and osmotic effects of NaCl-induced inactivation of Photosystems I and II in *Synechococcus* sp. *Plant Physiol* **123**: 1047-1056.
- Asada K, Heber U, Schreiber U. 1993.** Electron flow to the intersystem chain from stromal components and cyclic electron flow in maize chloroplasts, as detected in intact leaves by monitoring redox change of P700 and chlorophyll fluorescence. *Plant Cell Physiol* **34**(1): 39-50.
- Aslam SM, Patil PP, Vass I, Szabo M. 2022.** Heat-Induced Photosynthetic Responses of Symbiodiniaceae Revealed by Flash-Induced Fluorescence Relaxation Kinetics. *Frontiers in Marine Science* **9**.
- Björkman O, Demmig B. 1987.** Photon yield of O₂ evolution and chlorophyll fluorescence characteristics at 77 K among vascular plants of diverse origins. *Planta* **170**: 489-504.
- Blumwald E, Mehlhorn RJ, Packer L. 1983.** STUDIES OF OSMOREGULATION IN SALT ADAPTATION OF CYANOBACTERIA WITH ELECTRON-SPIN-RESONANCE SPIN-PROBE TECHNIQUES. *Proceedings of the National Academy of Sciences of the United States of America-Biological Sciences* **80**(9): 2599-2602.
- Cardona T, Sedoud A, Cox N, Rutherford AW. 2012.** Charge separation in Photosystem II: A comparative and evolutionary overview. *Biochim. Biophys. Acta* **1817**: 26-43.
- Crofts AR, Wraight CA. 1983.** The electrochemical domain of photosynthesis. *Biochim. Biophys. Acta* **726**: 149-185.
- Dabrowski P, Baczewska-Dabrowska AH, Bussotti F, Pollastrini M, Piekut K, Kowalik W, Wróbel J, Kalaji HM. 2021.** Photosynthetic efficiency of *Microcystis* ssp. under salt stress. *Environmental and Experimental Botany* **186**.
- Deák Z, Sass L, Kiss É, Vass I. 2014.** Characterization of wave phenomena in the relaxation of flash-induced chlorophyll fluorescence yield in cyanobacteria. *Biochim. Biophys. Acta* **1837**: 1522-1532.
- Demeter S, Vass I, Hideg É, Sallai A. 1985.** Comparative thermoluminescence study of triazine-resistant and -susceptible biotypes of *Erigeron canadensis* L. *Biochim. Biophys. Acta* **806**: 16-24.
- Diner BA, Schlodder E, Nixon PJ, Coleman WJ, Rappaport F, Lavergne J, Vermaas WFJ, Chisholm D. 2001.** Site-directed mutations at D1-His198 and D2-His197 of Photosystem II in *Synechocystis* PCC 6803: Sites of primary charge separation and cation and triplet stabilization. *Biochemistry* **40**: 9265-9281.
- Genty B, Briantais J-M, Baker NR. 1989.** The relationship between the quantum yield of photosynthetic electron transport and quenching of chlorophyll fluorescence. *Biochim. Biophys. Acta* **990**: 87-92.
- Gong H, Tang Y, Wang J, Wen X, Zhang L, Lu C. 2008.** Characterization of photosystem II in salt-stressed cyanobacterial *Spirulina platensis* cells. *Biochim. Biophys. Acta* **1777**: 488-495.
- Gotoh E, Kobayashi Y, Tsuyama M. 2010.** The post-illumination chlorophyll fluorescence transient indicates the RuBP regeneration limitation of photosynthesis in low light in *Arabidopsis*. *FEBS Letters* **584**(14): 3061-3064.

- Jeanjean R, Matthijs HCP, Onana B, Havaux M, Joset F. 1993.** Exposure of the cyanobacterium *Synechocystis* PCC6803 to salt stress induces concerted changes in respiration and photosynthesis. *Plant Cell Physiol* **34**: 1073-1079.
- Joset F, Jeanjean R, Hagemann M. 1996.** Dynamics of the response of cyanobacteria to salt stress: Deciphering the molecular events. *Physiologia Plantarum* **96**(4): 738-744.
- Kalaji HM, Jajoo A, Oukarroum A, Brestic M, Zivcak M, Samborska IA, Cetner MD, Lukasik I, Goltsev V, Ladle RJ. 2016.** Chlorophyll a fluorescence as a tool to monitor physiological status of plants under abiotic stress conditions. *Acta Physiologiae Plantarum* **38**(4).
- Kalaji HM, Schansker G, Ladle RJ, Goltsev V, Bosa K, Allakhverdiev SI, Bussotti F, Calatayud A, Dabrowski P, Elsheery N, et al. 2014.** Frequently asked questions about in vivo chlorophyll fluorescence: practical issues. *Photosynth. Res* **122**(2): 121-158.
- Kauny J, Setif P. 2014.** NADPH fluorescence in the cyanobacterium *Synechocystis* sp. PCC 6803: A versatile probe for *in vivo* measurements of rates, yields and pools. *Biochim. Biophys. Acta* **1837**(6): 792-801.
- Klughhammer C, Schreiber U. 1994.** An improved method, using saturating light pulses, for the determination of photosystem I quantum yield via P700⁺-absorbance changes at 830 nm. *Planta* **192**: 261-268.
- Krishna PS, Morello G, Mamedov F. 2019.** Characterization of the transient fluorescence wave phenomenon that occurs during H₂ production in *Chlamydomonas reinhardtii*. *Journal of Experimental Botany* **70**(21): 6321-6336.
- Kusama S, Miyake C, Nakanishi S, Shimakawa G. 2022.** Dissection of respiratory and cyclic electron transport in *Synechocystis* sp. PCC 6803. *Journal of Plant Research* **135**(4): 555-564.
- Lu C, Vonshak A. 2002.** Effects of salinity stress on photosystem II function in cyanobacterial *Spirulina platensis* cells. *Physiologia Plantarum* **114**(3): 405-413.
- Lu CM, Vonshak A. 1999.** Characterization of PSII photochemistry in salt-adapted cells of cyanobacterium *Spirulina platensis*. *New Phytologist* **141**(2): 231-239.
- Lu CM, Zhang JH. 1999.** Effects of salt stress on PSII function and photoinhibition in the cyanobacterium *Spirulina platensis*. *Journal of Plant Physiology* **155**(6): 740-745.
- Mano J, Miyake C, Schreiber U, Asada K. 1995.** Photoactivation of the electron flow from NADPH to plastoquinone in spinach chloroplasts. *Plant Cell Physiol* **36**(8): 1589-1598.
- Mi H, Endo T, Ogawa T, Asada K. 1995.** Thylakoid membrane-bound, NADPH-specific pyridine nucleotide dehydrogenase complex mediates cyclic electron transport in the cyanobacterium *Synechocystis* sp. PCC 6803. *Plant Cell Physiol* **36**(4): 661-668.
- Miller AG, Canvin DT. 1989.** GLYCOALDEHYDE INHIBITS CO₂ FIXATION IN THE CYANOBACTERIUM SYNECHOCOCCUS UTEX-625 WITHOUT INHIBITING THE ACCUMULATION OF INORGANIC CARBON OR THE ASSOCIATED QUENCHING OF CHLOROPHYLL A FLUORESCENCE. *Plant Physiology* **91**(3): 1044-1049.
- Pan T, Liu MM, Kreslavski VD, Zharmukhamedov SK, Nie CR, Yu M, Kuznetsov VV, Allakhverdiev SI, Shabala S. 2021.** Non-stomatal limitation of photosynthesis by soil salinity. *Critical Reviews in Environmental Science and Technology* **51**(8): 791-825.
- Patil PP, Vass I, Kodru S, Szabo M. 2020.** A multi-parametric screening platform for photosynthetic trait characterization of microalgae and cyanobacteria under inorganic carbon limitation. *Plos One* **15**(7).

- Patil PP, Vass I, Szabó M. 2022.** Characterization of the Wave Phenomenon in Flash-Induced Fluorescence Relaxation and Its Application to Study Cyclic Electron Pathways in Microalgae. *International Journal of Molecular Sciences* **23**(9).
- Rehman AU, Cser K, Sass L, Vass I. 2013.** Characterization of singlet oxygen production and its involvement in photodamage of Photosystem II in the cyanobacterium *Synechocystis* PCC 6803 by histidine-mediated chemical trapping. *Biochim. Biophys. Acta* **1827**: 689-698.
- Robinson HH, Crofts A. 1983.** Kinetics of the oxidation-reduction reactions of the Photosystem II quinone acceptor complex, and the pathway for deactivation. *FEBS Lett* **153**: 221-226.
- Schiewer U, Erdmann N, Kuhnke KH. 1978.** INFLUENCE OF DIFFERENT NACL CONCENTRATIONS ON PHOTOSYNTHETIC INTENSITY OF BLUE-GREEN-ALGAE MICROCYSTIS-FIRMA AND SYNECHOCYSTIS-AQUATILIS. *Biochemie Und Physiologie Der Pflanzen* **172**(4): 351-368.
- Schreiber U 2004.** Pulse-Amplitude-Modulation (PAM) fluorometry and saturation pulse method: an overview. *Chlorophyll a Fluorescence*. Netherlands: Springer, 279-319.
- Schreiber U, Klughammer C. 2009.** New NADPH/9-AA module for the DUAL-PAM-100: Description, operation and examples of application. *PAM Application Notes* **2**: 1-13.
- Schreiber U, Klughammer C, Kolbowski J. 2012.** Assessment of wavelength-dependent parameters of photosynthetic electron transport with a new type of multi-color PAM chlorophyll fluorometer. *Photosynthesis Research* **113**(1-3): 127-144.
- Schubert H, Hagemann M. 1990.** SALT EFFECTS ON 77K FLUORESCENCE AND PHOTOSYNTHESIS IN THE CYANOBACTERIUM SYNECHOCYSTIS SP PCC-6803. *Fems Microbiology Letters* **71**(1-2): 169-172.
- Shikanai T, Endo T, Hashimoto T, Yamada Y, Asada K, Yokota A. 1998.** Directed disruption of the tobacco *ndhB* gene impairs cyclic electron flow around Photosystem I. *Proc. Natl. Acad. Sci. USA* **95**: 9705-9709.
- Sudhir P, Murthy SDS. 2004.** Effects of salt stress on basic processes of photosynthesis. *Photosynthetica* **42**(4): 481-486.
- Sudhir PR, Pogoryelov D, Kovács L, Garab G, Murthy SDS. 2005.** The effects of salt stress on photosynthetic electron transport and thylakoid membrane proteins in the cyanobacterium *Spirulina platensis*. *Journal of Biochemistry and Molecular Biology* **38**(4): 481-485.
- Szabo M, Larkum AWD, Suggett DJ, Vass I, Sass L, Osmond B, Zavafer A, Ralph PJ, Chow WS. 2017.** Non-intrusive Assessment of Photosystem II and Photosystem I in Whole Coral Tissues. *Frontiers in Marine Science* **4**: 12.
- Trtilek M, Kramer DM, Koblizek M. 1997.** Dual-modulation LED kinetic fluorometer. *J. Lumin* **72-74**: 597-599.
- Vass I, Cook KM, Deák Z, Mayes SR, Barber J. 1992.** Thermoluminescence and flash-oxygen characterization of the IC2 deletion mutant of *Synechocystis* sp. PCC 6803 lacking the Photosystem II 33 kDa protein. *Biochim. Biophys. Acta* **1102**: 195-201.
- Vass I, Horvath G, Herczeg T, Demeter S. 1981.** Photosynthetic energy conservation investigated by thermoluminescence. Activation energies and half-lives of thermoluminescence bands of chloroplasts determined by mathematical resolution of glow curves. *Biochim. Biophys. Acta* **634**: 140-152.
- Vass I, Kirilovsky D, Etienne A-L. 1999.** UV-B radiation-induced donor- and acceptor-side modifications of Photosystem II in the cyanobacterium *Synechocystis* sp. PCC 6803. *Biochemistry* **38**: 12786-12794.
- Vass I, Ono TA, Inoue Y. 1987.** Removal of 33 kDa extrinsic protein specifically stabilizes the S₂Q_A- charge pair in Photosystem II. *FEBS Lett* **211**: 215-220.

- Yang WJ, Wang F, Liu LN, Sui N. 2020.** Responses of Membranes and the Photosynthetic Apparatus to Salt Stress in Cyanobacteria. *Frontiers in Plant Science* **11**: 10.
- Yang XH, Liang Z, Wen XG, Lu CM. 2008.** Genetic engineering of the biosynthesis of glycinebetaine leads to increased tolerance of photosynthesis to salt stress in transgenic tobacco plants. *Plant Mol Biol* **66**(1-2): 73-86.
- Zeng MT, Vonshak A. 1998.** Adaptation of *Spirulina platensis* to salinity-stress. *Comparative Biochemistry and Physiology a-Molecular & Integrative Physiology* **120**(1): 113-118.
- Zhang T, Gong HM, Wen XG, Lu CM. 2010.** Salt stress induces a decrease in excitation energy transfer from phycobilisomes to photosystem II but an increase to photosystem I in the cyanobacterium *Spirulina platensis*. *Journal of Plant Physiology* **167**(12): 951-958.